Copy No. _____

Defence Research and Development Canada
Recherche et développement pour la défense Canada

DEFENCE R&D DÉFENSE

Magnetic Source Parameters of *MR OFFSHORE* Measured During Trial MONGOOSE 07

J. Bradley Nelson
Troy C. Richards

Defence R&D Canada – Atlantic

Technical Memorandum
DRDC Atlantic TM 2007-223
September 2007

Canada

This page intentionally left blank.

Magnetic Source Parameters of *MR OFFSHORE* Measured During Trial MONGOOSE 07

J. Bradley Nelson and Troy C. Richards

Defence R&D Canada – Atlantic

Technical Memorandum 2007-223

September 2007

Author

Original signed by Troy C. Richards

J. Bradley Nelson and Troy C. Richards

Approved by

Original signed by Dave Hopkin

Dave Hopkin

H/Signatures

Approved for release by

Original signed by James L. Kennedy

James L. Kennedy

DRP Chair

Abstract

Sea mines can be triggered by the magnetic field from a naval vessel, and thus monitoring the magnetic state of a naval vessel is critical. The vessel's signature is usually measured by sailing it over an electromagnetic (EM) range equipped with bottom-mounted magnetic sensors. If the magnetic signature is too large, then some type of treatment (degaussing, de-perming, etc) is done to reduce it. Range facilities are often far from the vessel's operating area and require considerable transit time to reach them. "Forward EM ranging" is the term used for making EM signature measurements with portable sensors while the vessel is in the operating area.

One concept for locating and identifying sea mines is to use a combined sonar/magnetic detection system. The Naval Surface Warfare Center in Panama City, Florida (NSWC-PC) has developed such a system on a REMUS autonomous underwater vehicle (AUV). Because the REMUS magnetic sensor is also capable of measuring a naval vessel's signature, and its navigation system is capable of measuring the AUV's position and orientation, then it should be possible to use their REMUS for forward EM ranging.

DRDC Atlantic and NSWC-PC measured the magnetic signature of the vessel *MR OFFSHORE* using the laser scalar magnetic gradiometer-equipped REMUS underwater vehicle during trial MONGOOSE 07 in June 2007. The magnetic signatures were measured on a number of ship and REMUS headings. These data have been analysed to yield the permanent and induced magnetic parameters of *MR OFFSHORE*. Two different modeling techniques, one using dipoles and quadrupoles, and another using a single prolate spheroid, were used and the results are consistent.

The DRDC Diver Signature Integrated Measurement System (DSIMS) was deployed on the sea-bottom during trial MONGOOSE 07. It contained electric, magnetic, acoustic, and pressure sensors and was used primarily to assess the vulnerability of divers to sea mines during typical MCM operations. However, it was also used to measure the magnetic signals from *MR OFFSHORE* on one ship pass directly over top of the DSIMS sensors. The prolate spheroid parameters obtained from the REMUS data were used to predict the 3-component signature of *MR OFFSHORE* during this pass. The fit was quite close, and the estimated speed of the ship based on the fitting algorithm matched the captain's declared speed during the pass. This validates the concept of using mobile surface magnetic sensors to predict magnetic signatures beneath the ship.

Résumé

Les mines marines peuvent être déclenchées par le champ magnétique d'un navire de guerre. C'est pourquoi il est critique de surveiller l'état magnétique d'un navire de guerre. La signature d'un navire est normalement mesurée lorsque le navire passe au-dessus d'installations d'essais électromagnétiques (EM) munies de détecteurs magnétiques de fond. Si la signature magnétique est d'une dimension trop grande, une certaine forme de traitement (démagnétisation, démagnétisation permanente ou autre) y est appliquée en vue de sa réduction. Les installations d'essais EM sont souvent éloignées de la zone de manœuvre du navire, et il faut compter un temps de transit considérable pour y parvenir. « Essais EM en zone avancée » désigne la prise de mesures de signatures EM à l'aide de capteurs portatifs lorsque le navire se trouve dans la zone de manœuvre.

Un système de détection magnétique/sonar combiné sert à la localisation et à l'identification des mines marines. Le Naval Surface Warfare Center (NSWC-PC), à Panama City (Floride), a mis au point un tel système à bord du véhicule sous-marin autonome (AUV) REMUS. Comme le REMUS est muni d'un capteur magnétique qui peut aussi mesurer la signature d'un navire de guerre et que son système de navigation peut mesurer sa position et son orientation, il devrait alors être possible de se servir du REMUS aux fins d'essais EM avancés.

RDDC Atlantique et le NSWC-PC ont mesuré la signature magnétique du navire MR OFFSHORE à l'aide du REMUS muni d'un gradiomètre magnétique scalaire laser durant l'essai MONGOOSE 2007, en juin 2007. Les signatures magnétiques ont été mesurées pour un certain nombre de caps du navire et du REMUS. Les données ont été analysées pour donner les paramètres magnétiques induits et permanents du MR OFFSHORE. On a utilisé deux techniques de modélisation, dont l'une fait appel à des doublets et à des quadripôles et l'autre, à un sphéroïde étendu, et les résultats sont uniformes.

Le système intégré de mesure de signatures de plongeur (SIMSP) de RDDC a été déployé sur le fond de la mer durant l'essai MONGOOSE 2007. Muni de capteurs électriques, magnétiques, acoustiques et de pression, il a servi principalement à l'évaluation de la vulnérabilité des plongeurs aux mines marines durant des opérations typiques de lutte contre les mines (LCM). Il a cependant aussi servi à la mesure des signaux magnétiques du MR OFFSHORE lors d'un passage du navire directement au-dessus des capteurs SIMSP. Les paramètres du sphéroïde étendu obtenus à partir des données fournies par le REMUS ont servi à la prédiction de la signature à trois composants du MR OFFSHORE durant ce passage. L'ajustement était assez fin, et la vitesse estimée du navire fondée sur l'algorithme de réglage a correspondu à la vitesse déclarée par le capitaine durant le passage, ce qui valide le concept d'utilisation de capteurs magnétiques mobiles de surface pour la prédiction des signatures magnétiques au-dessous du navire.

Executive summary

Background:

Sea mines can be triggered by the magnetic field from a naval vessel, and thus monitoring the magnetic state of a naval vessel is critical. "Forward EM ranging" is the term used for making electromagnetic signature measurements with portable sensors while the vessel is in the operating area. The Naval Surface Warfare Center in Panama City, Florida (NSWC-PC) has installed a combined sonar/magnetic detection system on a REMUS autonomous underwater vehicle (AUV) to detect sea mines. The REMUS magnetic sensor is also capable of measuring a naval vessel's signature, and its navigation system is capable of measuring the AUV's position and orientation. Thus it should be possible to use their system for forward EM ranging.

DRDC Atlantic and NSWC-PC measured the magnetic signature of the vessel *MR OFFSHORE* using the laser scalar magnetic gradiometer-equipped REMUS underwater vehicle during trial MONGOOSE 07 in June 2007. The magnetic signatures were measured on a number of ship and REMUS headings. These data have been analysed to yield the permanent and induced magnetic properties of *MR OFFSHORE*.

Results:

Two different models were used to analyse the data: an 18-term model consisting of permanent and induced dipoles and quadrupoles; and a single prolate spheroid with permanent and induced magnetization. In the 18-term model, the position of sources is allowed to vary while in the prolate spheroid model, the position is fixed at the midpoint of the ship. The dipole parameters of the two models agree very well although the actual quality of the fit is somewhat better with the 18-term model.

The DRDC Diver Signature Integrated Measurement System (DSIMS) was deployed on the sea-bottom during trial MONGOOSE 07. It contained electric, magnetic, acoustic, and pressure sensors and was used primarily to assess the vulnerability of divers to sea mines during typical MCM operations. However, it was also used to measure the magnetic signals from *MR OFFSHORE* on one ship pass directly over top of the DSIMS sensors. The prolate spheroid parameters obtained from the REMUS data were used to predict the 3-component signature of *MR OFFSHORE* during this pass. The fit was quite close, and the estimated speed of the ship based on the fitting algorithm matched the captain's declared speed during the pass.

The biggest problem with the analysis was due to the poor quality of the REMUS position data. Jumps and steps in the GPS data made it difficult to determine the correct position of the magnetometers. Although planned, a more detailed analysis of the effect of the ship's motion on the recorded signals was not undertaken.

Significance:

The close match between the predicted and measured 3-component near-field signature of *MR OFFSHORE* on the DSIMS pass validates the concept of using mobile surface magnetic sensors

to predict magnetic signatures beneath the ship. This could be a core component of a forward EM range capability.

Future Work:

Future work on using magnetometer-equipped vehicles for forward EM ranging will require better positioning data for the vehicle. This may entail using differentially-corrected GPS instead of Ca-Code GPS data, as well as the use orientation sensors.

The AUV traveled very slowly on the surface of the ocean during this experiment. It may be more practical to tow the sensors behind a zodiac to increase the number of runs which can be performed in a given time. A data set with at least 16 runs in total, collected on four ship headings, with good vehicle position data would allow a more detailed investigation of the robustness of the various parameter estimates.

The ship orientation data should be collected on future experiments to determine if the pitching and rolling motion has a significant impact on the measured signatures, and thus on the parameter estimates.

Trials with a degaussed vessel, which will have a much more complex magnetic signature, must be performed to confirm the technique is applicable to naval vessels in a forward area.

Nelson, JB, and Richards, TC, 2007. Magnetic Source Parameters of *MR OFFSHORE* Measured During Trial MONGOOSE 07. DRDC Atlantic TM 2007-223. Defence Research and Development Canada – Atlantic.

Sommaire

Introduction

Les mines marines peuvent être déclenchées par le champ magnétique d'un navire de guerre. C'est pourquoi il est critique de surveiller l'état magnétique d'un navire de guerre. « Essais EM en zone avancée » est l'expression dont on se sert pour désigner la prise de mesures de signatures EM à l'aide de capteurs portatifs lorsque le navire visé se trouve dans la zone de manœuvre. Le Naval Surface Warfare Center (NSWC-PC), à Panama City (Floride), a installé un système de détection magnétique/sonar combiné à bord d'un véhicule sous-marin autonome (AUV) REMUS pour détecter les mines marines. Le REMUS est muni d'un capteur magnétique qui peut aussi mesurer la signature d'un navire de guerre, et son système de navigation peut mesurer sa position et son orientation. Il devrait alors être possible de se servir du REMUS aux fins d'essais EM en zone avancée.

RDDC Atlantique et le NSWC-PC ont mesuré la signature magnétique du navire *MR OFFSHORE* à l'aide du REMUS muni d'un gradiomètre magnétique scalaire laser durant l'essai MONGOOSE 2007, en juin 2007. Les signatures magnétiques ont été mesurées pour un certain nombre de caps du navire et du REMUS. Les données ont été analysées pour donner les paramètres magnétiques induits et permanents du *MR OFFSHORE*.

Résultats

Deux modèles ont servi à l'analyse des données : un modèle de 18 termes, composé de doublets et de quadripôles permanents et induits; et un sphéroïde étendu à aimantation permanente et induite. Dans le modèle de 18 termes, la position des sources peut varier, tandis que, dans le sphéroïde étendu, la position est fixe au point intermédiaire du navire. Les paramètres des doublets des deux modèles concordent très bien, mais la qualité réelle de l'ajustement est légèrement supérieure dans le cas du modèle de 18 termes.

Le système intégré de mesure de signatures de plongeur (SIMSP) de RDDC a été déployé sur le fond de la mer durant l'essai MONGOOSE 2007. Muni de capteurs électriques, magnétiques, acoustiques et de pression, il a servi principalement à l'évaluation de la vulnérabilité des plongeurs aux mines marines durant des opérations normales de lutte contre les mines (LCM). Il a cependant aussi servi à la mesure des signaux magnétiques du *MR OFFSHORE* lors d'un passage du navire directement au-dessus des capteurs SIMSP. Les paramètres du sphéroïde étendu obtenus à partir des données fournies par le REMUS ont servi à la prédiction de la signature à trois composants du *MR OFFSHORE* durant ce passage. L'ajustement était assez fin, et la vitesse estimée du navire fondée sur l'algorithme de réglage a correspondu à la vitesse déclarée par le capitaine durant le passage.

Le principal problème rattaché à l'analyse était attribuable à la mauvaise qualité des données sur la position fournies par le REMUS. Des augmentations marquées et par paliers des données GPS ont rendu difficile la détermination de la position correcte des magnétomètres. Même si une analyse détaillée des effets des mouvements du navire sur les signaux enregistrées avait été prévue, elle n'a pas été menée.

Portée

La forte concordance entre les valeurs prédites et mesurées de la signature à trois composants en champ proche du *MR OFFSHORE* lors du passage à proximité du SIMSP valide le concept de l'utilisation de capteurs magnétiques mobiles de surface pour la prédiction des signatures magnétiques au-dessous d'un navire, ce qui pourrait constituer un élément de base d'une capacité d'essai EM avancé.

Recherches futures

Pour que des recherches soient menées à une date ultérieure au sujet de l'utilisation de véhicules munis de magnétomètres aux fins d'essais EM en zone avancée, il faudra disposer de meilleures données sur la position à l'égard des véhicules, ce qui pourrait donner lieu à l'utilisation de données GPS en mode différentiel au lieu de données GPS code Ca, ainsi qu'à l'utilisation de capteurs d'orientation.

L'AUV s'est déplacé très lentement à la surface de l'océan durant l'expérience. Il pourrait s'avérer plus pratique de remorquer les capteurs à l'aide d'un canot pneumatique de type Zodiac pour augmenter le nombre de parcours qu'il est possible d'effectuer dans un délai donné. Une série de données recueillies au cours d'au moins 16 parcours à l'égard de quatre caps de navire, assortie de bonnes données sur la position du véhicule, permettrait des examens plus détaillés de la robustesse des estimations des divers paramètres.

Des données sur l'orientation du navire devraient être recueillies au cours de recherches à une date ultérieure pour permettre de déterminer si le tangage et le roulis ont une incidence significative sur les signatures mesurées et, par conséquent, les estimations des paramètres.

Il faut mener des essais à l'aide d'un navire démagnétisé, dont la signature magnétique est beaucoup plus complexe, pour confirmer si la technique peut s'appliquer aux navires de guerre dans une zone avancée.

Nelson, JB, and Richards, TC, 2007. *Magnetic Source Parameters of MR OFFSHORE Measured During Trial MONGOOSE 07* (paramètres des sources magnétiques du MR OFFSHORE mesurés durant l'essai MONGOOSE 2007). DRDC Atlantic TM 2007-223. Defence R&D Canada – Atlantic.

Table of contents

List of figures

List of tables

1. Introduction

Sea mines can be triggered by the magnetic field from a naval vessel, and thus monitoring the magnetic state of a naval vessel is critical. "Forward EM ranging" is the term used for making electromagnetic signature measurements with portable sensors while the vessel is in the operating area. The essential elements of any such system are:

1) a magnetic sensor
2) vessel-sensor relative position measurements.

In order to determine if the magnetic fields from the ship might trigger a sea mine, it is necessary to either measure those fields beneath the ship, or measure the fields at other positions and then predict what the fields would be beneath the ship. In order to make accurate predictions, many measurements must be taken at many points in space. Several options are available for obtaining such measurements:

1) use a large array of sensors and have the ship make a single pass, thus obtaining all measurements at once,
2) use a small array of sensors and have the ship make several passes by the sensors, or
3) use a mobile sensor and make several passes by the ship.

The third option was investigated in this work.

The Naval Surface Warfare Center in Panama City, Florida (NSWC-PC) has developed combined sonar/magnetic detection system on a REMUS autonomous underwater vehicle (AUV) for mine detection. The magnetic sensor, called the laser scalar gradiometer (LSG), consists of four Helium^3 magnetometers configured in such a way as to measure the total magnetic field and the (X,Y,Z) spatial gradients of the total field. The magnetic sensor is manufactured by Polatomic. The navigation system consists of a GPS and an inertial navigation system (INS). When the vehicle is on the surface, the position is taken from GPS. When the vehicle is underwater, the system takes the last good GPS fix and double integrates the inertial data to determine the position. In all cases, the vehicle's orientation is measured with the INS. The REMUS vehicle is also equipped with vector magnetometers for modeling and reducing the magnetic noise on the LSG signals. Figure 1 shows the REMUS vehicle.

The LSG is a very low-noise magnetic sensor so clearly the first criterion of a forward range is met. If the REMUS is operated only on the surface then there are GPS position data for the magnetic sensor. The vessel's position and orientation can be measured with multiple GPS systems, or a combined GPS/INS system, so the second criterion can be met. Consequently it should be possible to use the LSG-equipped REMUS vehicle as a forward EM ranging platform for a naval vessel.

Figure 1. The NSWC-PC REMUS autonomous underwater vehicle.

Figure 2. Desired REMUS track for a given ship heading. Note this drawing is not to scale.

DRDC Atlantic and NSWC-PC measured the magnetic signature of the vessel *MR OFFSHORE* using the laser scalar magnetic gradiometer-equipped REMUS during trial MONGOOSE 07 in June 2007. *MR OFFSHORE* was equipped with an integrated GPS/INS made by the National Research Council of Canada. All REMUS and *MR OFFSHORE* data were time-tagged with universal time (UTC).

Two REMUS passes were made on each ship heading as shown in Figure 2. Three ship headings were used, yielding a total of 6 passes in all. Figure 3 shows the combined *MR OFFSHORE* and REMUS tracks during the entire trial.

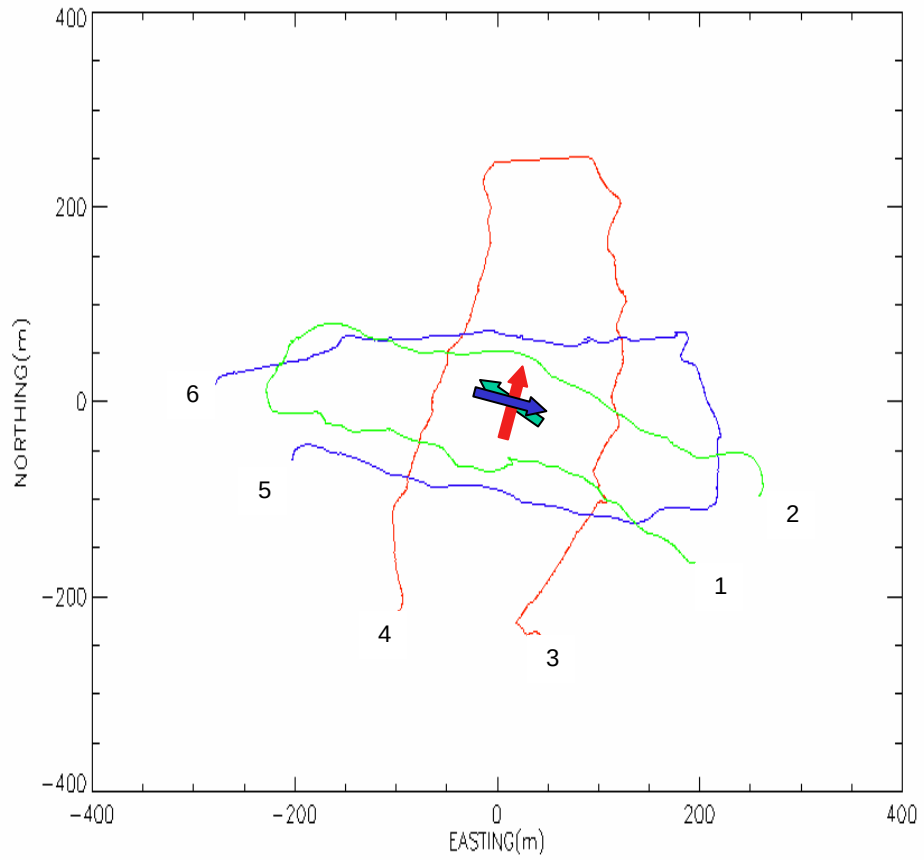

Figure 3. Relative position of REMUS vs MR OFFSHORE for all passes. Arrows indicate the three ship headings. Pass numbers are indicated at the ends of each line.

2. Magnetic models used in this analysis

In this section we use the convention that normal font denotes scalar quantities, bold font denotes vector quantities, and underlined bold font denotes tensor quantities.

The magnetic field (**B**) is a vector quantity, but the total field (TF'), which is the amplitude of the magnetic field, is a scalar. It is given by:

$$TF' = \sqrt{B_x{}^2 + B_y{}^2 + B_z{}^2} \quad . \tag{1}$$

Consider the situation where there is a small magnetic field due to a ship ($\mathbf{B_{ship}}$ with amplitude B_{ship}) perturbing the Earth's background magnetic field ($\mathbf{B_{earth}}$ with amplitude B_{earth}). Further, let us assume that the ship's magnetic field is much smaller than the Earth's magnetic field

$$\left| B_{ship} \right| << \left| B_{earth} \right| \quad . \tag{2}$$

Therefore

$$TF' = \sqrt{(B_{earthX} + B_{shipX})^2 + (B_{earthY} + B_{shipY})^2 + (B_{earthY} + B_{shipY})^2}$$

$$= \sqrt{\begin{array}{l} (B_{earthX}{}^2 + 2B_{earthX}B_{shipX} + B_{shipX}{}^2) + \\ (B_{earthY}{}^2 + 2B_{earthY}B_{shipY} + B_{shipY}{}^2) + \\ (B_{earthZ}{}^2 + 2B_{earthZ}B_{shipZ} + B_{shipZ}{}^2) \end{array}} \tag{3}$$

Rearranging terms gives

$$TF' = \sqrt{\begin{array}{l} (B_{earthX}{}^2 + B_{earthY}{}^2 + B_{earthZ}{}^2) + \\ 2(B_{earthX}B_{shipX} + B_{earthY}B_{shipY} + B_{earthZ}B_{shipZ}) + \\ (B_{shipX}{}^2 + B_{shipY}{}^2 + B_{shipZ}{}^2) \end{array}}$$

$$= \sqrt{B_{earth}{}^2 + 2(\mathbf{B_{earth}} \bullet \mathbf{B_{ship}}) + B_{ship}{}^2}$$

$$= B_{earth}\sqrt{1 + 2(\mathbf{B_{earth}} \bullet \mathbf{B_{ship}}) / B_{earth}{}^2 + (B_{ship} / B_{earth})^2} \quad . \tag{4}$$

Because the ship's field is much less than the Earth's filed, we can neglect the last term. Taking the binomial expansion of the remaining terms gives

$$TF' = B_{earth}\,[1 + 2(\mathbf{B_{earth}} \cdot \mathbf{B_{ship}})/\,(2B_{earth}{}^2)]$$

$$= B_{earth} + (\mathbf{B_{earth}} \cdot \mathbf{B_{ship}})/ B_{earth}$$

$$= B_{earth} + (\mathbf{B_e} \cdot \mathbf{B_{ship}}) \quad (5)$$

or $$TF = TF' - B_{earth} = (\mathbf{B_e} \cdot \mathbf{B_{ship}}) \quad (6)$$

where TF is defined as the total-field anomaly due to the ship and $\mathbf{B_e}$ is a unit vector in the direction of the Earth's field. Thus the total-field perturbation caused by the ship is given by the projection of the ship's actual magnetic field ($\mathbf{B_{ship}}$) along the direction of the background magnetic field ($\mathbf{B_e}$).

2.1 18-term dipole/quadrupole model

Ships have many sources of static magnetic fields including the ferrous materials in the hull and machinery, electrical currents flowing in the electronics, corrosion currents, etc. Previous experiments with *CFAV QUEST* (Ref 1-3) suggest that in order to get a robust model for the ship's sources, one must account for the induced and permanent dipole and quadrupole moments. In addition, trends and offsets in the Earth's field from one pass to another must be accounted for. The model used in those references is

$$TF = DC + Trend + (TF_{MP} + TF_{MI}) + (TF_{QP} + TF_{QI}) \quad (7)$$

where the subscripts "MP" refer to permanent dipole, "MI" to induced dipole, "QP" to permanent quadrupole, and "QI" to induced quadrupole. Let us use the ship's coordinate system for all calculations ("x" = forward, "y" = starboard, and "z" = down). Unit vectors in these directions are denoted **i**, **j**, and **k** respectively.

The equation for the magnetic field due to a magnetic dipole is (Ref 4, page 218)

$$\mathbf{B} = \frac{\mu_0}{4\pi}\left\{\frac{3\mathbf{R}(\mathbf{m} \bullet \mathbf{R})}{R^5} - \frac{\mathbf{m}}{R^3}\right\} \quad . \quad (8)$$

Combining equations (8) and (6) yields the total-field anomaly due to the dipole moment of a ship measured in the presence of the Earth's background magnetic field

$$TF = \frac{\mu_0}{4\pi}\left\{\frac{3(\mathbf{m} \bullet \mathbf{R})(\mathbf{R} \bullet \mathbf{B_e})}{R^5} - \frac{\mathbf{m} \bullet \mathbf{B_e}}{R^3}\right\} \quad (9)$$

where $\mu_o = 4\pi \times 10^{-7}$,
m is the total dipole moment vector, in Ampere·metre^2,
$\mathbf{B_e}$ is a unit vector in the direction of the Earth's magnetic field, and
R is the vector from the source dipole to the magnetometer in metres,

Thus

$$\mathbf{R} = (x-x_0)\mathbf{i} + (y-y_0)\mathbf{j} + (z-z_0)\mathbf{k} \quad (10a)$$

and $$R = \sqrt{(x - x_0)^2 + (y - y_0)^2 + (z - z_0)^2} \quad . \tag{10b}$$

where (x,y,z) is the position of the measurement point, and (x_0,y_0,z_0) is the position of the dipole. The total dipole moment vector is comprised of the following components:

- longitudinal permanent dipole moment (m_{Px}) (11a)
- transverse permanent dipole moment (m_{Py}) (11b)
- vertical permanent dipole moment (m_{Pz}) (11c)
- longitudinal induced dipole moment (m_{Ix}) (11d)
- transverse induced dipole moment (m_{Iy}) (11e)
- vertical induced dipole moment (m_{Iz}) . (11f)

The longitudinal and transverse induced dipole moments change with heading but the vertical induced dipole moment does not. Thus we usually refer to just the total vertical dipole moment given by

$$m_z = m_{Pz} + m_{Iz} \quad . \tag{12a}$$

The horizontal induced dipole moments are given by:

$$m_{Ix} = C_x B_{ex} W \tag{12b}$$
$$m_{Iy} = C_y B_{ey} W \tag{12c}$$

where W is the tonnage of the vessel, B_{ex} is the longitudinal component of the Earth's magnetic field, B_{ey} is the transverse component of the Earth's magnetic field, and C_x and C_y are coefficients determined by the shape of the vessel and the magnetic susceptibility of the steel. The position of the induced and permanent dipoles is assumed to be at $(\Delta x, \Delta y, \Delta z)$ relative to the measured position of the vessel (in most cases this will be relative to the GPS antenna on the ship). Thus there are eight unknowns for the magnetic dipole model (m_{Px}, m_{Py}, m_z, C_x, C_y, Δx, Δy, and Δz).

In Ref 1 it was shown that the number of unknowns can be reduced if we assume that the centre of the permanent and induced dipoles lies at $\Delta y = 0$ (this is a reasonable assumption if the GPS antenna is positioned along the mid-line of the ship) and if C_x is simply related to C_y . A prolate spheroid with a semi-major axis of 18 metres and a semi-minor axis of 5.32 metres was chosen to fit the geometry of *CFAV QUEST* in Ref 3, yielding:

$$C_y / C_x = 0.22 \quad . \tag{13}$$

The same ratio was used for *MR OFFSHORE* in this work. Thus there are 6 terms that account for the permanent and induced magnetic dipoles (m_{Px}, m_{Py}, m_z, C_x, Δx, and Δz).

The full equations for the total-magnetic field due to a quadrupole are derived in Annex A. Again we can break up the total quadrupole moment into the permanent $\underline{\mathbf{Q_P}}$ and induced $\underline{\mathbf{Q_I}}$. The position of the quadrupole is assumed to be the same as that of the magnetic dipole. After rearranging terms, we get the following terms for the total-field due to a permanent quadrupole moment:

$$TF_{QP} = (-\mu_0/8\pi)\{B_{ex}Term_{Px} + B_{ey}Term_{Py} + B_{ez}Term_{Pz}\} \quad . \qquad (15)$$

where

$$\begin{aligned} Term_{Px} = {} & Q_{Pxx}[\,(5(x-x_0)^3/R^7) - (5(x-x_0)(z-z_0)^2/R^7) - (2(x-x_0)/R^5)\,] + \\ & Q_{Pxy}[\,(10(x-x_0)^2(y-y_0)/R^7) - (2(y-y_0)/R^5)\,] + \\ & Q_{Pxz}[\,(10(x-x_0)^2(z-z_0)/R^7) - (2(z-z_0)/R^5)\,] + \\ & Q_{Pyy}[\,(5(x-x_0)(y-y_0)^2/R^7) - (5(x-x_0)(z-z_0)^2/R^7)\,] + \\ & Q_{Pyz}[\,(10(x-x_0)(y-y_0)(z-z_0)/R^7)\,] \quad . \end{aligned} \qquad (16a)$$

$$\begin{aligned} Term_{Py} = {} & Q_{Pxx}[\,(5(x-x_0)^2(y-y_0)/R^7) - (5(y-y_0)(z-z_0)^2/R^7)\,] + \\ & Q_{Pxy}[\,(10(x-x_0)(y-y_0)^2/R^7) - (2(x-x_0)/R^5)\,] + \\ & Q_{Pxz}[\,(10(x-x_0)(y-y_0)(z-z_0)/R^7)\,] + \\ & Q_{Pyy}[\,(5(y-y_0)^3/R^7) - (5(y-y_0)(z-z_0)^2/R^7) - (2(y-y_0)/R^5)\,] + \\ & Q_{Pyz}[\,(10(y-y_0)^2(z-z_0)/R^7) - (2(z-z_0)/R^5)\,] \quad . \end{aligned} \qquad (16b)$$

$$\begin{aligned} Term_{Pz} = {} & Q_{Pxx}[\,(5(x-x_0)^2(z-z_0)/R^7) - (5(z-z_0)^3/R^7) + (2(z-z_0)/R^5)\,] + \\ & Q_{Pxy}[\,(10(x-x_0)(y-y_0)(z-z_0)/R^7)\,] + \\ & Q_{Pxz}[\,(10(x-x_0)(z-z_0)^2/R^7) - (2(x-x_0)/R^5)\,] + \\ & Q_{Pyy}[\,(5(y-y_0)^2(z-z_0)/R^7) - (5(z-z_0)^3/R^7) + (2(z-z_0)/R^5)\,] + \\ & Q_{Pyz}[\,(10(y-y_0)(z-z_0)^2/R^7) - (2(y-y_0)/R^5)\,] \end{aligned} \qquad (16c)$$

The induced quadrupole is assumed to be co-located with the permanent quadrupole.

$$TF_{QI} = (-\mu_0/8\pi)\{B_{ex}Term_{Ix} + B_{ey}Term_{Iy} + B_{ez}Term_{Iz}\} \quad . \qquad (17)$$

$$\begin{aligned} Term_{Ix} = {} & Q_{Pxx}B_{ex}B_{ex}[\,(5(x-x_0)^3/R^7) - (5(x-x_0)(z-z_0)^2/R^7) - (2(x-x_0)/R^5)\,] + \\ & Q_{Pxy}B_{ex}B_{ey}[\,(10(x-x_0)^2(y-y_0)/R^7) - (2(y-y_0)/R^5)\,] + \\ & Q_{Pxz}B_{ex}B_{ez}[\,(10(x-x_0)^2(z-z_0)/R^7) - (2(z-z_0)/R^5)\,] + \\ & Q_{Pyy}B_{ey}B_{ey}[\,(5(x-x_0)(y-y_0)^2/R^7) - (5(x-x_0)(z-z_0)^2/R^7)\,] + \\ & Q_{Pyz}B_{ey}B_{ez}[\,(10(x-x_0)(y-y_0)(z-z_0)/R^7)\,] \quad . \end{aligned} \qquad (18a)$$

$$\begin{aligned} Term_{Iy} = {} & Q_{Pxx}B_{ex}B_{ex}[\,(5(x-x_0)^2(y-y_0)/R^7) - (5(y-y_0)(z-z_0)^2/R^7)\,] + \\ & Q_{Pxy}B_{ex}B_{ey}[\,(10(x-x_0)(y-y_0)^2/R^7) - (2(x-x_0)/R^5)\,] + \\ & Q_{Pxz}B_{ex}B_{ez}[\,(10(x-x_0)(y-y_0)(z-z_0)/R^7)\,] + \\ & Q_{Pyy}B_{ey}B_{ey}[\,(5(y-y_0)^3/R^7) - (5(y-y_0)(z-z_0)^2/R^7) - (2(y-y_0)/R^5)\,] + \\ & Q_{Pyz}B_{ey}B_{ez}[\,(10(y-y_0)^2(z-z_0)/R^7) - (2(z-z_0)/R^5)\,] \quad . \end{aligned} \qquad (18b)$$

$$\begin{aligned} Term_{Iz} = {} & Q_{Pxx}B_{ex}B_{ex}[\,(5(x-x_0)^2(z-z_0)/R^7) - (5(z-z_0)^3/R^7) + (2(z-z_0)/R^5)\,] + \\ & Q_{Pxy}B_{ex}B_{ey}[\,(10(x-x_0)(y-y_0)(z-z_0)/R^7)\,] + \\ & Q_{Pxz}B_{ex}B_{ez}[\,(10(x-x_0)(z-z_0)^2/R^7) - (2(x-x_0)/R^5)\,] + \\ & Q_{Pyy}B_{ey}B_{ey}[\,(5(y-y_0)^2(z-z_0)/R^7) - (5(z-z_0)^3/R^7) + (2(z-z_0)/R^5)\,] + \\ & Q_{Pyz}B_{ey}B_{ez}[\,(10(y-y_0)(z-z_0)^2/R^7) - (2(y-y_0)/R^5)\,] \quad . \end{aligned} \qquad (18c)$$

Thus there are 10 terms that account for the induced and permanent quadrupole moments. If we assume that the centre of the quadrupoles and the GPS antenna are both along the mid-line of the ship, as we did for the dipoles, then $y_0 = 0$.

Finally, the background geology and low-frequency geomagnetic variations were modeled as a DC offset and trend for each pass. Thus an 18-term model was developed for the ship's total-field with the following unknowns:

m_{Px}, m_{Py}, m_z
C_x, (C_y = 0.22 x C_x)
Δx, Δz (Δy=0; sources and GPS antenna lie along the mid-line of the ship)
Q_{Pxx}, Q_{Pxy}, Q_{Pxz}, Q_{Pyy}, Q_{Pyz}
Q_{Ixx}, Q_{Ixy}, Q_{Ixz}, Q_{Iyy}, Q_{Iyz}
DC offset and Trend for each pass .

2.2 Prolate spheroid model

Figure 4 shows a prolate spheroid with semi-major axis "a" and semi-minor axis "b".

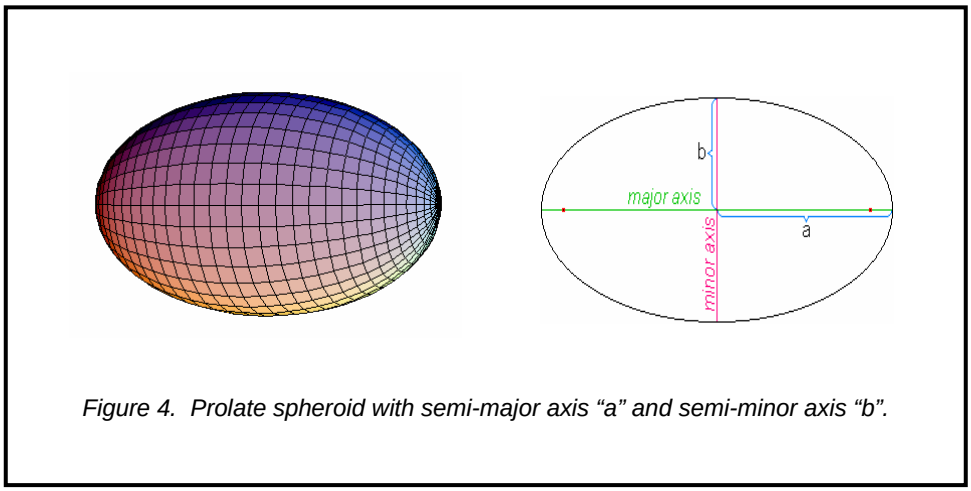

Figure 4. Prolate spheroid with semi-major axis "a" and semi-minor axis "b".

In this case, we assume that the ship can be modeled as a single prolate spheroid with permanent magnetization $\mathbf{M_P}$ and induced magnetization $\mathbf{M_I}$, both in Ampere/metre. The permanent magnetization has the components (M_{Px}, M_{Py}, M_{Pz}), and the induced magnetization is a function of the geometry of the prolate spheroid and the magnetic susceptibility χ_m, a dimensionless parameter given by (Ref 5, pages 172-173):

$$\chi_m = \mu_r - 1 \qquad (19)$$

where μ_r is the relative permeability of the prolate spheroid material. The components of the induced magnetization in a prolate spheroid are:

$$M_{Ix} = H_X \chi_m/(1+N_X \chi_m) \ , \qquad (20a)$$
$$M_{Iy} = H_Y \chi_m/(1+N_Y \chi_m) \ , \qquad (20b)$$
$$M_{Iz} = H_Z \chi_m/(1+N_Z \chi_m) \ , \qquad (20c)$$

where N_i is the demagnetization factor and H_i is the inducing field (in A/m) in the i^{th} direction. Due to symmetry, $N_Z = N_Y$. The demagnetization factors are:

$$N_X = (\xi_0^{\,2} - 1)[\frac{\xi_0}{2}\log_n(\frac{\xi_0 + 1}{\xi_0 - 1}) - 1] \tag{21a}$$

$$N_Y = N_Z = \frac{\xi_0^{\,2}}{2} - \frac{\xi_0(\xi_0^{\,2} - 1)}{4}\log_n(\frac{\xi_0 + 1}{\xi_0 - 1}) \tag{21b}$$

where
$$\xi_0 = \frac{a}{\sqrt{a^2 - b^2}} \quad . \tag{22}$$

At large distances from a uniformly magnetized prolate spheroid the magnetic field is that of a magnetic dipole, given by

$$\mathbf{m} = \mathbf{M}V \tag{23}$$

where V, the volume, is given by

$$V = \frac{4\pi ab^2}{3} . \tag{24}$$

At small distances, however, the magnetic field is not purely dipolar and the exact equations are derived in Annex B and also available in Ref 6.

The single prolate spheroid model assumed that its position is known exactly. This is in contrast to the 18-term model of Section 2.1 which explicitly allowed the position of the dipole and quadrupole to vary ($\Delta x, \Delta z$). The centre of the prolate spheroid was chosen to be the centre of the ship which, in this experiment, was some 18.96 m to the stern of the GPS antenna. The vertical position of the prolate spheroid was chosen at 1.5 m above the waterline of the ship.

The fitting routine also allowed for DC offsets and trends on each pass. Thus the unknown parameters in the prolate spheroid model were:

M_{Px}, M_{Py}, M_{Pz}
χ_m
DC offset and Trend for each pass .

Table 1 gives the various parameters used in both magnetic models of *MR OFFSHORE*, and information on the experimental conditions.

Table 1. Various parameters used in computing the model parameters, and conditions for the experiment.

PARAMETER	VALUE
MR OFFSHORE length	37.92 m
MR OFFSHORE beam	7.82 m
Tonnage	200 tonnes
Semi-major axis “a”	18.96 m
Semi-minor axis “b”	3.91 m
ξ_o	18.55 m
N_x	0.05822
$N_y = N_z$	0.47089
B_{North}	24061 nT
B_{East}	-1117 nT
B_{Down}	41964 nT
H_{North}	19.147 A/m
H_{East}	0.8889 A/m
H_{Down}	33.394 A/m
Approximate ship headings	305°, 15°, 105° Magnetic
Sea state	50 cm waves, slight chop, very little swell
Time required per pass	8-10 minutes
Typical REMUS speed during passes	1.5 knots (0.75 m/s)

3. Data

The AUV navigation data were sampled at 1 Hz. The AUV magnetic data were sampled at 430 Hz and decimated to 43 Hz by NSWC-PC personnel. The ship navigation data were sampled at 10 Hz and decimated to 1 Hz.

The AUV and ship horizontal position data were inspected for bad values and corrected as necessary. The ship navigation data were very good, but the REMUS position data had several single-point glitches and steps of several metres. The glitches were easily corrected, but it was not clear how to correct the steps (which data were valid, those prior to, or after, the step?). We tried removing all steps but this actually led to worse fits so, in the end, we left them in. The ship and AUV vertical position were set to zero as both were (nominally) on the surface of the ocean during this experiment.

The AUV and ship pitch, roll, and heading data were visually inspected and bad values were corrected as necessary. Again the ship orientation data were excellent and required very little correction but the REMUS data were significantly worse. Splines were used to interpolate over bad or missing data but many of these segments lasted for several seconds. The REMUS inertial data was intended to be used only for noise reduction. However, it was determined that sufficient noise reduction could be obtained using only the vector magnetometers and thus the REMUS inertial data were not actually used in this analysis.

The total-field and vector magnetometer data from the LSG, but not the spatial gradients, were used in this analysis. These data had no glitches or steps and required no corrections. The DC component of the total field (48386 nT) was subtracted to yield the quantity “TF”. The AUV magnetic noise was modeled with the same 18-term noise model used in aircraft noise reduction (Ref 7), where the terms were derived from the vector magnetometers signals and their derivatives. This noise was subtracted from TF yielding the compensated total-field “TFC”. TFC was used in all the subsequent analysis. Annex C describes the process for removing the AUV manoeuvre noise and Figure 5 compares the raw (TF) and compensated (TFC) total-field signals.

Finally, TFC and the vector magnetometer data were sub-sampled to 1 Hz and time aligned with the ship and AUV navigation data.

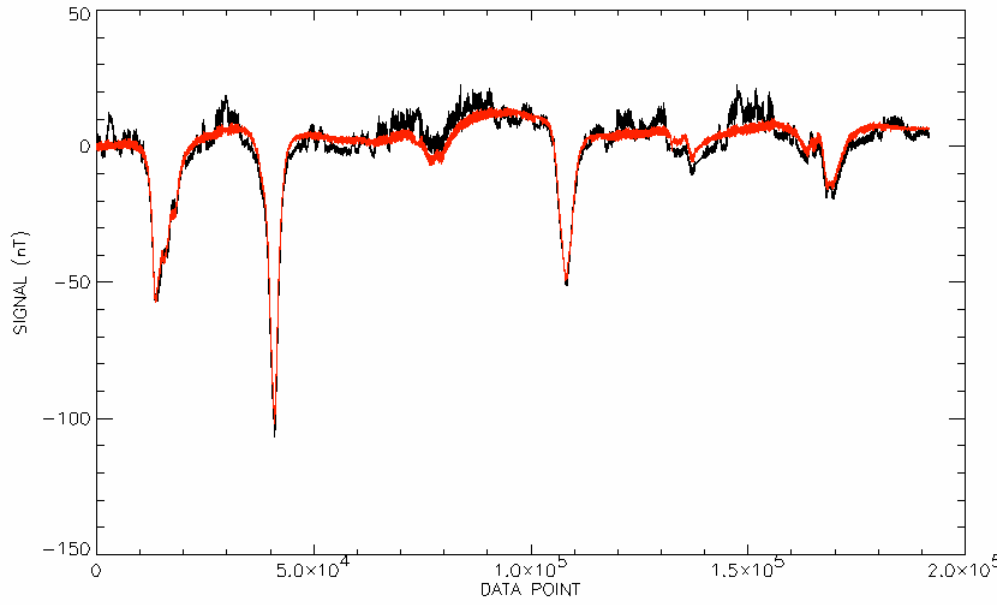

Figure 5. Raw total-field (TF, black) vs compensated total-field (TFC, red) for all six passes.

4. Results

4.1 18-term dipole/quadrupole model

Figure 6 compares TFC to the best fit and residual using the 18-term dipole/quadrupole model. Notice the large residual in the first signature near data point 280. This corresponds to a discontinuity in the AUV navigation data described in Section 3. The discontinuity can be seen in the lower green trace in Figure 3 (Easting ~ 0; Northing ~ -70). The parameters that result from fitting all 6 passes to the dipole/quadrupole model are given in Section 4.2.

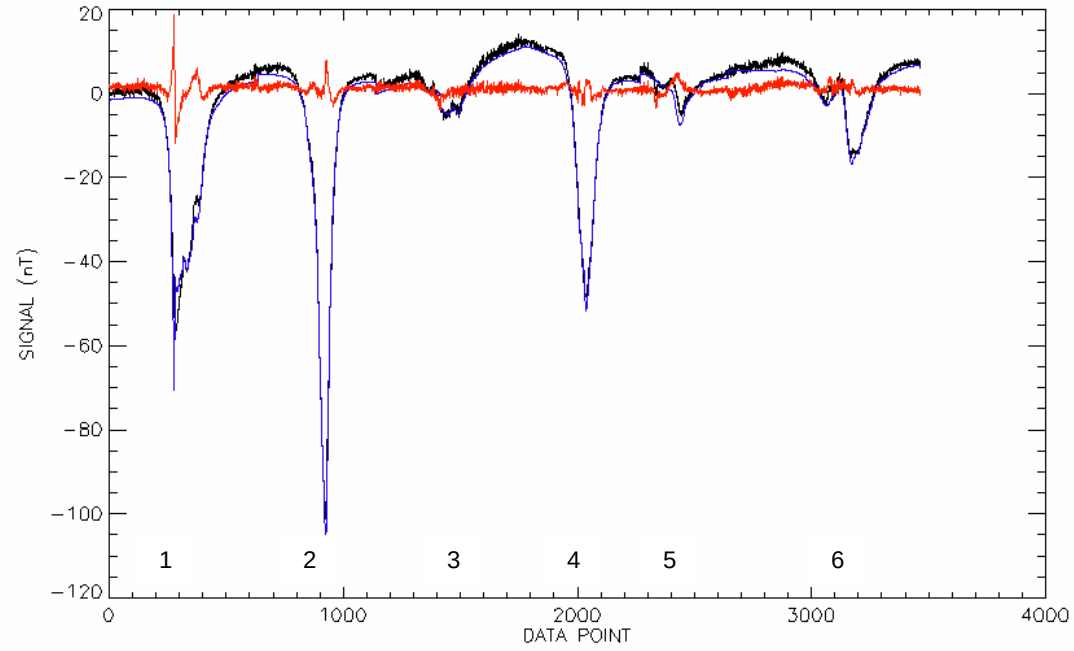

Figure 6. TFC (black) vs. best-fit with 18-term model (blue) vs. residual (red) for all six passes. The pass numbers are shown at the bottom and correspond to the numbers shown in Figure 3.

4.2 Single prolate spheroid model

Figure 7 compares TFC to the best fit and residual using the single prolate spheroid model.

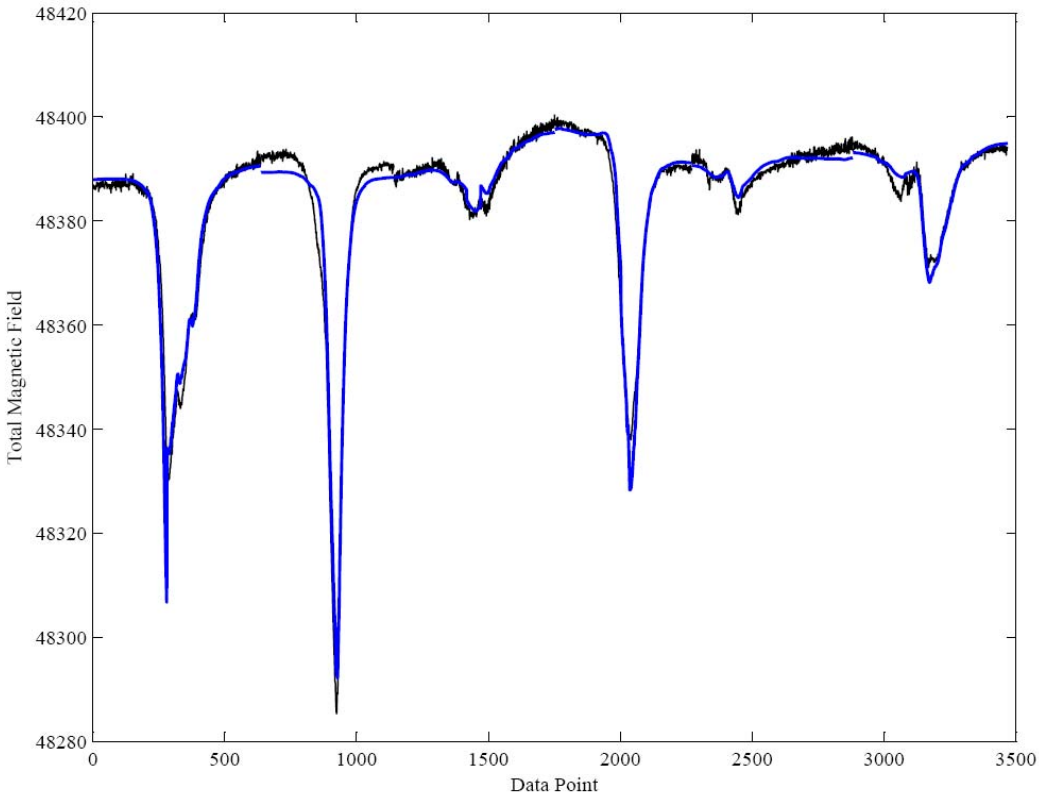

Figure 7. TFC (black) vs. best-fit with a single prolate spheroid (blue) for all six passes. Note the Earth's field = 48386 nT has been added to TFC for the prolate spheroid modeling.

Tables 2 and 3 compare the estimates of the parameters obtained using the dipole/quadrupole and prolate spheroid models. Although the two models use different parameters, they can be related to each other using the equations given in Sections 2.1 and 2.2, and the values in Table 1.

Table 2. Comparison of best-fit source parameters for the two models using units of Am^2 for dipole moment and $Am^2/nT/tonne$ for C_x .

MODEL	m_{Px} (10^5 Am^2)	m_{Py} (10^5 Am^2)	m_z (10^5 Am^2)	C_x ($Am^2/nT/tonne$)	Δx (m)	Δz (m)	$\sigma_{Residual}$ (nT)
18-term	0.54	-0.33	1.20	0.93	-15.7	-2.2	1.48
Prolate Spheroid	0.66	-0.34	1.08	0.68	-19.0	-1.5	2.93

Table 3. Comparison of best-fit source parameters for the two models using units of A/m for magnetization and dimensionless units for χ_m .

MODEL	M_{Px} (A/m)	M_{Py} (A/m)	M_z (A/m)	χ_m	Δx (m)	Δz (m)	$\sigma_{Residual}$ (nT)
18-term	44.5	-27.2	98.8	2.11	-15.7	-2.2	1.48
Prolate Spheroid	54.0	-28.3	88.6	1.54	-19.0	-1.5	2.93

4.3 Single prolate spheroid model used to predict *MR OFFSHORE* signatures collected with DSIMS

DRDC's Diver Signature Integrated Measurement System (DSIMS) was also deployed during Trial MONGOOSE 07. This system contains pressure, acoustic, electric-field, and magnetic-field sensors. A full description can be found in Ref 8-10. *MR OFFSHORE* made a single pass over top of the DSIMS sensor array and, even though the ship's position data were not recorded, it was possible to estimate the ship's 3-component signature. The ship's heading and the position, and the orientation of the DSIMS vector magnetometers were known. The ship was assumed to have gone directly over the DSIMS sensors. The time of closest-point-of-approach and speed were varied to find the best match to the measured signals. Table 4 gives the known parameters for the pass. Figure 8 compares the DSIMS measured signatures and the best-fit model using the parameters from the prolate spheroid model (Table 3) and the best-fit speed. It is interesting to note that the best-fit speed was 3.2 knots, which exactly matches the speed indicated by the ship's captain.

Although the fit is not perfect, it certainly is close enough to indicate that the prolate spheroid parameters derived from surface measurements can be used to predict the magnetic signature beneath the ship.

Table 4 .Parameters for the MR OFFSHORE pass near the DSIMS sensor array.

PARAMETER	VALUE
Ship heading	90°True
Ship speed	3.2 knots (1.6 m/s)
Sensor depth	10.2 m
Sensor Orientation	North, East, Down (True)
Ship offset	0 m (assumed)
Vertical position of prolate spheroid	1.5 m above waterline (assumed)

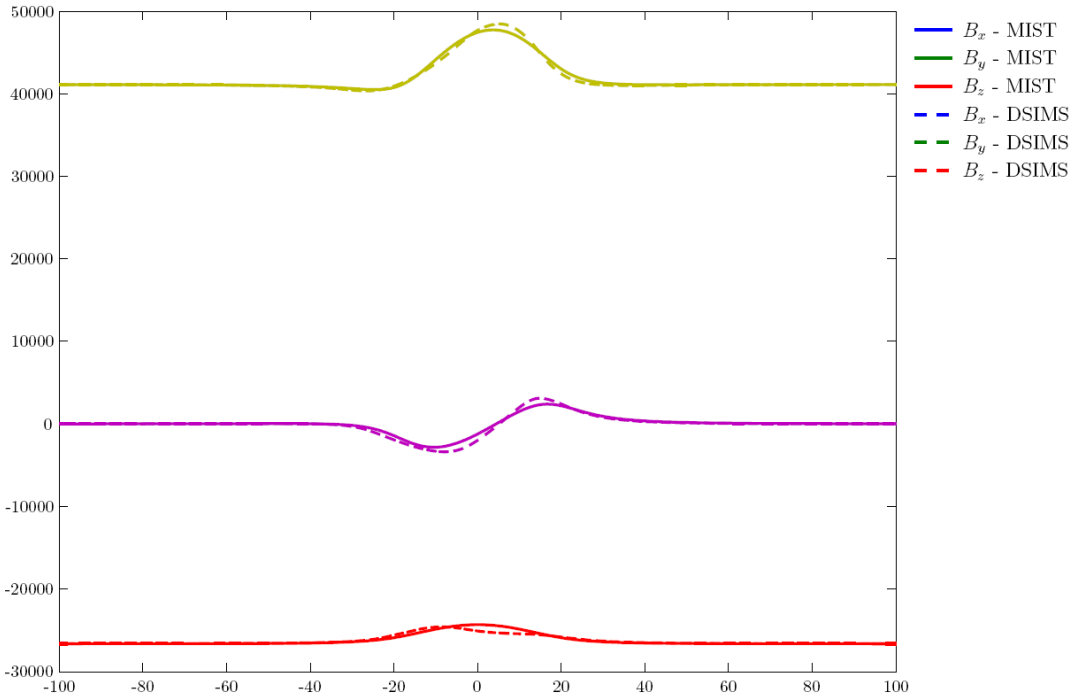

Figure 8. Comparison of predicted vs. measured MR OFFSHORE 3-component signature during pass by DSIMS sensor package. The prolate spheroid model was used in this prediction. "MIST indicates predicted signals and DSIMS indicates measured values.

5. Conclusions

The largest source of error in inverting the measured magnetic signatures into source parameters was the poor quality of the REMUS position data. The authors could not adequately remove the DC shifts in both the latitude and longitude data because it was unclear which data (before the shift or after it?) were valid and which needed correction.

The objective of collecting the ship orientation information was to determine if the pitching and rolling of the ship during the runs made a significant difference to the signatures, and thus to the parameter estimates. This analysis was not attempted because of the problems with the REMUS navigation data described above.

Tables 2 and 3 indicate that the magnetic parameters obtained from the two different models are quite consistent. The longitudinal permanent dipole moment, and magnetization, derived from the two models agree to within roughly 20%. The transverse permanent dipole moment, or magnetization, from the two models agree to within 3%. The total vertical dipole moments, or magnetizations, agree to within roughly 10%. The longitudinal susceptibility coefficient C_x, or magnetic susceptibility χ_m, agree to within roughly 25%. The position of the best-fit dipole/quadrupole in the 18-term model is very close to the centre of the ship. Thus, given the problems with the navigation data, this should be considered as quite reasonable agreement between the two models.

The prolate spheroid model parameters were used to successfully predict the 3-components of *MR OFFSHORE*'s near-field magnetic signature as measured by the DSIMS sensor package. This validates the concept of using mobile surface magnetic sensors to predict magnetic signatures beneath the ship. This could be a core component of a forward EM range capability.

The LSG-equipped REMUS is clearly capable of measuring ship magnetic signatures, but two shortcomings were evident in this trial. The first problem is the poor quality of the REMUS position data. In order to use magnetometer-equipped UAVs as forward magnetic ranging systems, it is imperative that better quality data be obtained because even small errors in the position data cause large errors in the fits at close ranges. The second problem relates to the time required to conduct the trial. The REMUS vehicle could not be driven on the surface under manual control, even in calm seas, at speeds >2 knots (for this experiment the average speed was only 1.5 knots). In heavy seas, this is a serious limitation.

6. Future work

Future work on using magnetometer-equipped vehicles for forward EM ranging will require better positioning data for the vehicle. This may entail using differentially-corrected GPS instead of Ca-Code GPS data, as well as the use orientation sensors.

The AUV traveled very slowly on the surface of the ocean during this experiment. It may be more practical to tow the sensors behind a zodiac to increase the number of runs which can be performed in a given time. A data set with at least 16 runs in total, collected on four ship headings, with good vehicle position data would allow a more detailed investigation of the robustness of the various parameter estimates.

The ship orientation data should be collected on future experiments to determine if the pitching and rolling motion has a significant impact on the measured signatures, and thus on the parameter estimates.

Trials with a degaussed vessel, which will have a much more complex magnetic signature, must be performed to confirm the technique is applicable to naval vessels in a forward area.

7. References

1. J. Bradley Nelson, *Magnetic Source Parameters for CFAV QUEST Calculated from Airborne MAD Measurements and Implications for Signature Management*, DRDC Atlantic TM 2003-234, November 2003.

2. J. Bradley Nelson, *Magnetic Source Parameters for CFAV QUEST During Trial Q281*, DRDC Atlantic TM 2004-144, June 2005.

3. J. Bradley Nelson, *Magnetic Source Parameters of CFAV QUEST: August 2005*, DRDC Atlantic TM 2006-002, January 2006.

4. Alan M. Portis, *Electromagnetic Fields Sources and Media*, John Wiley and Sons, New York, 1978.

5. Erik V. Bohn, *Introduction to Electromagnetic Fields and Waves*, Addison-Wesley Publishing Co, Menlo Park, California, USA, 1968.

6. Peter M. Holtham and Carmen E. Lucas, *New Approaches to Magnetic Modelling I. Prolate Spheroids II. One-Spike-at-a-Time Fitting*, Defence Research Establishment Pacific TM 93-81, November 1993.

7. J. Bradley Nelson, *An Improved Aeromagnetic Data Acquisition System for the NRC Convair 580*, NRC LTR-FR-170, November 2000.

8. Troy C. Richards, *DSIMS Operations Guide to International Dive Exercise DIVE 05*, DRDC Atlantic TM 2005-215, 2005.

9. Duane Watson, *Diver Signature Integrated Measurement System (DSIMS) Signal Transmission Upgrades*, DRDC Atlantic CR 2007-047, prepared for Troy Richards, 2007.

10. Dan Hutt, *1GO Thrust Completion Report*, DRDC Atlantic Technical Memorandum, in preparation.

Annex A: Derivation of the total magnetic field from a magnetic quadrupole in Cartesian coordinates

In general the magnetic field is related to the magnetic scalar potential by

$$\mathbf{B} = -\mathbf{Grad}(\Phi_M) \tag{A.1}$$

where in Cartesian coordinates the gradient operator is

$$\mathbf{Grad} = (\partial / \partial \mathrm{x})\mathbf{i} + (\partial / \partial \mathrm{y})\mathbf{j} + (\partial / \partial \mathrm{z})\mathbf{k} \ . \tag{A.2}$$

The magnetic scalar potential from a magnetic quadrupole is (Ref 5, page 229)

$$\Phi_M = \frac{\mu_0}{8\pi} \frac{\mathbf{R} \bullet \underline{\mathbf{Q}} \bullet \mathbf{R}}{\mathrm{R}^5} \tag{A.3}$$

where $\underline{\mathbf{Q}}$ is the total quadrupole moment tensor, in Ampere·metre^4, and
$\mathbf{R}$ is the vector from the source quadrupole to the measurement point in metres.

In Cartesian coordinates

$$\mathbf{R} = (\mathrm{x} - \mathrm{x}_0)\mathbf{i} + (\mathrm{y} - \mathrm{y}_0)\mathbf{j} + (\mathrm{z} - \mathrm{z}_0)\mathbf{k} \tag{A.4}$$

and

$$\underline{\mathbf{Q}} = \begin{bmatrix} \mathrm{Q_{XX}}\mathbf{ii} + \mathrm{Q_{XY}}\mathbf{ij} + \mathrm{Q_{XZ}}\mathbf{ik} \\ \mathrm{Q_{YX}}\mathbf{ji} + \mathrm{Q_{YY}}\mathbf{jj} + \mathrm{Q_{YZ}}\mathbf{jk} \\ \mathrm{Q_{ZX}}\mathbf{ki} + \mathrm{Q_{ZY}}\mathbf{kj} + \mathrm{Q_{ZZ}}\mathbf{kk} \end{bmatrix} \ . \tag{A.5}$$

The quadrupole tensor is both symmetric and traceless so

$$\mathrm{Q_{AB}} = \mathrm{Q_{BA}} \tag{A.6}$$

and

$$\mathrm{Q_{ZZ}} = -(\mathrm{Q_{XX}} + \mathrm{Q_{YY}}) \ . \tag{A.7}$$

Thus

$$\frac{\mathbf{R} \bullet \underline{\mathbf{Q}} \bullet \mathbf{R}}{\mathrm{R}^5} = \frac{\mathbf{R}}{\mathrm{R}^5} \bullet \begin{bmatrix} \mathrm{Q_{XX}}\mathbf{ii} + \mathrm{Q_{XY}}\mathbf{ij} + \mathrm{Q_{XZ}}\mathbf{ik} \\ \mathrm{Q_{YX}}\mathbf{ji} + \mathrm{Q_{YY}}\mathbf{jj} + \mathrm{Q_{YZ}}\mathbf{jk} \\ \mathrm{Q_{ZX}}\mathbf{ki} + \mathrm{Q_{ZY}}\mathbf{kj} + \mathrm{Q_{ZZ}}\mathbf{kk} \end{bmatrix} \bullet \left[(\mathrm{x} - \mathrm{x}_0)\mathbf{i} + (\mathrm{y} - \mathrm{y}_0)\mathbf{j} + (\mathrm{z} - \mathrm{z}_0)\mathbf{k} \right]$$

$$= \frac{\mathbf{R}}{R^5} \bullet \begin{bmatrix} \{Q_{XX}(x - x_0) + Q_{XY}(y - y_0) + Q_{XZ}(z - z_0)\}\mathbf{i} + \\ \{Q_{YX}(x - x_0) + Q_{YY}(y - y_0) + Q_{YZ}(z - z_0)\}\mathbf{j} + \\ \{Q_{ZX}(x - x_0) + Q_{ZY}(y - y_0) + Q_{ZZ}(z - z_0)\}\mathbf{k} \end{bmatrix}$$

$$\begin{aligned} &= Q_{XX}\frac{(x - x_0)^2 - (z - z_0)^2}{R^5} + Q_{XY}\frac{2(x - x_0)(y - y_0)}{R^5} \\ &+ Q_{XZ}\frac{2(x - x_0)(z - z_0)}{R^5} + Q_{YY}\frac{(y - y_0)^2 - (z - z_0)^2}{R^5} \\ &+ Q_{YZ}\frac{2(y - y_0)(z - z_0)}{R^5} \end{aligned} \tag{A.8}$$

Thus

$$\begin{aligned} \Phi_M = \frac{\mu_0}{8\pi R^5}\{&Q_{XX}[(x - x_0)^2 - (z - z_0)^2] + Q_{XY}[2(x - x_0)(y - y_0)] \\ &+ Q_{XZ}[2(x - x_0)(z - z_0)] + Q_{YY}[(y - y_0)^2 - (z - z_0)^2] \\ &+ Q_{YZ}[2(y - y_0)(z - z_0)]\} \end{aligned} \tag{A.9}$$

Combining equations A.1, A.2, and A.9 gives

$$\begin{aligned} \mathbf{B} = -\frac{\mu_0}{8\pi}&[(\partial/\partial x)\mathbf{i} + (\partial/\partial y)\mathbf{j} + (\partial/\partial z)\mathbf{k}] \\ &[\{Q_{XX}[(x - x_0)^2 - (z - z_0)^2] + Q_{XY}[2(x - x_0)(y - y_0)] \\ &+ Q_{XZ}[2(x - x_0)(z - z_0)] + Q_{YY}[(y - y_0)^2 - (z - z_0)^2] \\ &+ Q_{YZ}[2(y - y_0)(z - z_0)]\}/R^5] \end{aligned} \tag{A.10}$$

To determine the total-field, we compute the partial derivatives in A.10 and take the dot product of **B** and a unit vector in the direction of the background Earth's magnetic field $\mathbf{B_e}$. This yields:

$$TF_Q = B_{ex}Term_X + B_{ey}Term_Y + B_{ez}Term_Z \ . \tag{A.11}$$

where

$$\begin{aligned} Term_X = (-\mu_0/8\pi)\{&Q_{XX}[(5(x-x_0)^3/R^7) - (5(x-x_0)(z-z_0)^2/R^7) - (2(x-x_0)/R^5)] + \\ &Q_{XY}[(10(x-x_0)^2(y-y_0)/R^7) - (2(y-y_0)/R^5)] + \\ &Q_{XZ}[(10(x-x_0)^2(z-z_0)/R^7) - (2(z-z_0)/R^5)] + \\ &Q_{YY}[(5(x-x_0)(y-y_0)^2/R^7) - (5(x-x_0)(z-z_0)^2/R^7)] + \\ &Q_{YZ}[(10(x-x_0)(y-y_0)(z-z_0)/R^7)]\} \ . \end{aligned} \tag{A.12}$$

$$\begin{aligned} Term_Y = (-\mu_0/8\pi)\{&Q_{XX}[(5(x-x_0)^2(y-y_0)/R^7) - (5(y-y_0)(z-z_0)^2/R^7)] + \\ &Q_{XY}[(10(x-x_0)(y-y_0)^2/R^7) - (2(x-x_0)/R^5)] + \end{aligned}$$

$$Q_{XZ}[\ (10(x-x_0)(y-y_0)(z-z_0)/R^7)\ ]\ +$$
$$Q_{YY}[\ (5(y-y_0)^3/R^7) - (5(y-y_0)(z-z_0)^2/R^7) - (2(y-y_0)/R^5)\ ]\ +$$
$$Q_{YZ}[\ (10(y-y_0)^2(z-z_0)/R^7) - (2(z-z_0)/R^5)\ ]\ \}\ . \qquad \text{(A.13)}$$

$$\text{Term}_Z = (-\mu_0/8\pi)\{Q_{XX}[\ (5(x-x_0)^2(z-z_0)/R^7) - (5(z-z_0)^3/R^7) + (2(z-z_0)/R^5)\ ]\ +$$
$$Q_{XY}[\ (10(x-x_0)(y-y_0)(z-z_0)/R^7)\ ]\ +$$
$$Q_{XZ}[\ (10(x-x_0)(z-z_0)^2/R^7) - (2(x-x_0)/R^5)\ ]\ +$$
$$Q_{YY}[\ (5(y-y_0)^2(z-z_0)/R^7) - (5(z-z_0)^3/R^7) + (2(z-z_0)/R^5)\ ]\ +$$
$$Q_{YZ}[\ (10(y-y_0)(z-z_0)^2/R^7) - (2(y-y_0)/R^5)\ ]\ \}\ . \qquad \text{(A.14)}$$

Annex B: Uniformly magnetized prolate spheroids

Prolate spheroids are volumes formed by revolving an ellipse around its major axes. For a uniformly magnetized prolate spheroid we consider two cases, the longitudinal case, where the magnetization is parallel to the axis of revolution, and the transverse case, where the magnetization is perpendicular to the axis revolution.

For this steady magnetic field problem we first review magnetostatics and then introduce prolate spheroidal coordinates. Solutions for the magnetic field of a prolate spheroid with both permanent and induced magnetizations are then derived.

Due to the algebraic burden associated with this problem use of modern symbolic algebra software which includes vector calculus operations, such as Maple is highly recommended. Maple worksheets of the following derivations are available upon request.

B.1 Magnetostatic review

Under the condition of a steady magnetic state and assuming no electrical currents are present, Maxwell's equations simplify to the magnetostatic case, described by the following two vector field equations

$$\boldsymbol{\nabla} \times \boldsymbol{H} = 0 \tag{B.1}$$

and

$$\boldsymbol{\nabla} \cdot \boldsymbol{B} = 0. \tag{B.2}$$

Where $\boldsymbol{H}$ is the magnetic field intensity in (A/m), $\boldsymbol{B}$ is the magnetic field in (T), and the curl ($\boldsymbol{\nabla}\times$) and divergence ($\boldsymbol{\nabla}\cdot$) operators are defined in their usual manner.

Any vector field with a curl of zero can be expressed as the gradient of a scalar potential and therefore the magnetic intensity can be written as

$$\boldsymbol{H} = -\boldsymbol{\nabla}\psi \tag{B.3}$$

where $\boldsymbol{\nabla}$ is the gradient operator and ψ is the scalar magnetic potential.

Uniformly magnetized spheroids can be considered as permanent magnets with a magnetization $\boldsymbol{M}$ existing inside the spheroid, and zero magnetization outside the spheroid. Adopting the notation that field values inside the spheroid are denoted with a 0 subscript, and field values outside the spheroid are demoted with a 1 subscript, the magnetic field inside the spheroid is given as

$$\boldsymbol{B}_0 = \mu_\circ \left(\boldsymbol{H}_0 + \boldsymbol{M}\right) \tag{B.4}$$

where $\mu_\circ$ is the magnetic permeability of free space and the magnetization is represented in the same units as the magnetic intensity. Substitution of (B.4) into (B.2), and using $\boldsymbol{H}_0 = -\boldsymbol{\nabla}\psi_0$ yields

$$\boldsymbol{\nabla}^2\psi_0 = -\boldsymbol{\nabla}\cdot\boldsymbol{M} \tag{B.5}$$

where $\boldsymbol{\nabla}^2 = \boldsymbol{\nabla} \cdot \boldsymbol{\nabla}$ is the Laplacian operator. When $\boldsymbol{M}$ is uniform as considered here $\boldsymbol{\nabla} \cdot \boldsymbol{M} = 0$ (except at the spheroid surface) and

$$\boldsymbol{\nabla}^2 \psi_0 = 0 \tag{B.6}$$

which is known as Laplace's equation for magnetostatics. On the surface of the spheroid there is a an abrupt change in $\boldsymbol{M}$ and (B.5) must be used. Outside of the spheroid $\boldsymbol{B}_1 = \mu_\circ \boldsymbol{H}_1$ since a constant magnetic permeability is assumed and we have $\boldsymbol{\nabla}^2 \psi_1 = 0$.

B.2 Prolate spheroidal coordinates

Problems involving the magnetic fields of a prolate spheroid are best solved by converting to a prolate spheroidal coordinate system, such as the one shown in Figure (B.1). We adopt the following mapping from prolate spheroidal coordinates (η, ξ, ϕ) to cartesian coordinates (x, y, z)

$$x = c\,\xi\eta \tag{B.7}$$
$$y = c\,\sqrt{(\xi^2 - 1)\,(1 - \eta^2)}\,\cos(\phi) \tag{B.8}$$
$$z = c\,\sqrt{(\xi^2 - 1)\,(1 - \eta^2)}\,\sin(\phi) \tag{B.9}$$

where $c = \sqrt{a^2 - b^2}$ is the focal length and a and b are the semi-major and semi-minor radii of the spheroid, with $a > b$. When $\xi = \xi_0$ is constant, the surface of a prolate spheroid is generated, with the ellipse revolving around the x-axis.

This choice of prolate spheroidal coordinates is identical to that defined by Stratton [4, p46], and matches the standard ship cartesian coordinate system, where x is the longitudinal axis, y is athwartships and z is positive down. The chosen axis order (η, ξ, ϕ) conforms to a right-handed coordinate system as seen in Figure (B.1).

By tedious manipulation, the inverse mapping is determined to be

$$\eta = \frac{1}{2c}\left(\sqrt{(x+c)^2 + y^2 + z^2} - \sqrt{(x-c)^2 + y^2 + z^2}\right) \tag{B.10}$$
$$\xi = \frac{1}{2c}\left(\sqrt{(x+c)^2 + y^2 + z^2} + \sqrt{(x-c)^2 + y^2 + z^2}\right) \tag{B.11}$$
$$\phi = \arctan\left(\frac{z}{y}\right), \tag{B.12}$$

which are defined on the following ranges

$$-1 \le \eta \le 1 \qquad 1 < \xi < \infty \qquad 0 \le \phi \le 2\pi. \tag{B.13}$$

To represent the magnetization of the spheroid as a magnetic moment $\boldsymbol{m}$ in $\left(\mathrm{Am}^2\right)$, the magnetization can be multiplied by the volume of the spheroid v in $\left(\mathrm{m}^3\right)$, such that $\boldsymbol{m} = \boldsymbol{M}\,v$. The volume of the spheroid generated when $\xi = \xi_0$, is given as

$$v = \frac{4\pi}{3} a\,b^2 \tag{B.14}$$
$$= \frac{4\pi}{3} c^3 \xi_0 \left(\xi_0^2 + 1\right). \tag{B.15}$$

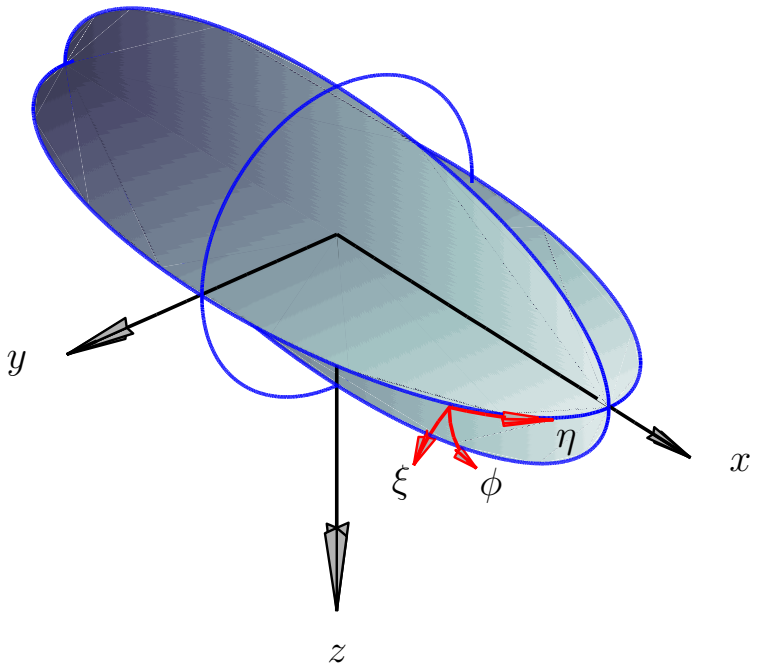

Figure B.1: Prolate spheroidal coordinates (η, ξ, ϕ) referenced to cartesian coordinates (x, y, z).

Note that both the magnetization and magnetic moment are vector quantities.

Using separation of variables, the general solution for Laplace's equation in prolate spheroidal coordinates is

$$\psi_1 = \sum_n \sum_m b_{m,n} P_n^m(\eta)\, Q_n^m(\xi)\, (e_m \sin(m\phi) + f_m \cos(m\phi)) \tag{B.16}$$

where P_n^m and Q_n^m are the associated Legendre functions of the 1st and 2nd kind, and $b_{m,n}, e_m$ and f_m are constants to be determined to match the boundary conditions ($\boldsymbol{B}$ normal and $\boldsymbol{H}$ tangential conserved) and satisfy finiteness of the solution.

B.3 Longitudinally magnetized prolate spheroid

A longitudinally magnetized prolate spheroid has a constant magnetization along the spheroid's axis of revolution, which is the x-axis in our chosen coordinate system. Such a magnetization can then be described as

$$\boldsymbol{M} = M_x\, \hat{\boldsymbol{a}}_x \tag{B.17}$$

where M_x is constant and $\hat{\boldsymbol{a}}_x$ is the unit vector in the x-direction. Inside the spheroid because the magnetization is constant the scalar magnetic potential will vary linearly with the x position and can be represented as

$$\psi_0 = N_x\, M_x\, x \tag{B.18}$$

where N_x is the longitudinal demagnetizing factor, a dimensionless constant which depends on the spheroid geometry. The magnetic field intensity inside the spheroid can be determined using (B.3) and is given as

$$\boldsymbol{H}_0 = -N_x\, M_x\ \hat{\boldsymbol{a}}_x. \tag{B.19}$$

For the magnetic field

$$\begin{aligned} \boldsymbol{B}_0 &= \mu_\circ \left(\boldsymbol{H}_0 + \boldsymbol{M}\right) && \text{(B.20)} \\ &= \mu_\circ \left(1 - \frac{1}{N_x}\right)\ \boldsymbol{H}_0. && \text{(B.21)} \end{aligned}$$

Transforming the magnetic intensity expression to prolate spheroidal coordinates we have

$$\boldsymbol{H}_0 = -N_x\, M_x \left(\frac{\sqrt{1-\eta^2}}{\sqrt{\xi^2-\eta^2}}\ \hat{\boldsymbol{a}}_\eta + \frac{\sqrt{\xi^2-1}}{\sqrt{\xi^2-\eta^2}}\ \hat{\boldsymbol{a}}_\xi\right). \tag{B.22}$$

Careful inspection of the general solution reveals that setting $m = 0, n = 1$ and $f_0 = 1$ will generate the correct functional form of the magnetic intensity to satisfy the boundary conditions. With these settings the general solution simplifies to a particular solution given as

$$\psi_1 = b_1 \eta \left(\frac{1}{2}\xi \ln\left(\frac{\xi+1}{\xi-1}\right) - 1\right). \tag{B.23}$$

The remaining unknowns b_1 and N_x are determined by matching the two boundary conditions,

$$H_{0\eta} = H_{1\eta} \tag{B.24}$$

and

$$\left(1 - \frac{1}{N_x}\right) H_{0\xi} = H_{1\xi}, \tag{B.25}$$

evaluated on the surface of the spheroid $\xi = \xi_0$. Solving the two simultaneous equations yields the longitudinal demagnetizing factor

$$N_x = \left(\xi_0^2 - 1\right)\left[\frac{\xi_0}{2} \ln\left(\frac{\xi_0+1}{\xi_0-1}\right) - 1\right]. \tag{B.26}$$

and

$$b_1 = c\, \xi_0 M_x \left(\xi_0^2 - 1\right). \tag{B.27}$$

The expressions for $\boldsymbol{B}$ and $\boldsymbol{H}$ both inside and outside the prolate spheroid are now known. In particular, for the magnetic intensity outside of the spheroid, converted back to cartesian coordinates, we arrive at

$$\begin{aligned} \boldsymbol{H}_1 &= M_x \xi_0 \left(\xi_0^2 - 1\right) \left\{ \left(\frac{\xi}{\xi^2-\eta^2} - \frac{1}{2} \ln\left(\frac{\xi_0+1}{\xi_0-1}\right)\right) \hat{\boldsymbol{a}}_x \right. \\ &\quad \left. + \frac{\eta \cos(\phi)\sqrt{1-\eta^2}}{\left(\xi^2-\eta^2\right)\sqrt{\xi^2-1}}\, \hat{\boldsymbol{a}}_y + \frac{\eta \sin(\phi)\sqrt{1-\eta^2}}{\left(\xi^2-\eta^2\right)\sqrt{\xi^2-1}}\, \hat{\boldsymbol{a}}_z \right\}. \end{aligned}$$

The magnetic field outside the prolate spheroid is given as $\boldsymbol{B}_1 = \mu_\circ \boldsymbol{H}_1$.

B.4 Transversely magnetized prolate spheroid

A transversely magnetized prolate spheroid has a constant magnetization perpendicular to the spheroid's axis of revolution. Such a magnetization, for our example, can be described as

$$\boldsymbol{M} = M_y \, \hat{\boldsymbol{a}}_y \tag{B.28}$$

where M_y is constant and $\hat{\boldsymbol{a}}_y$ is the unit vector in the y-direction. Inside the spheroid because the magnetization is constant the scalar magnetic potential will vary linearly with the y position and can be represented as

$$\psi_0 = N_y \, M_y \, y \tag{B.29}$$

where N_y is the transverse demagnetizing factor, a dimensionless constant which depends on the spheroid geometry. The magnetic field intensity inside the spheroid can be determined using (B.3) and is given as

$$\boldsymbol{H}_0 = -N_y \, M_y \; \hat{\boldsymbol{a}}_y. \tag{B.30}$$

For the magnetic field

$$\begin{aligned} \boldsymbol{B}_0 &= \mu_\circ \left(\boldsymbol{H}_0 + \boldsymbol{M} \right) && \text{(B.31)} \\ &= \mu_\circ \left(1 - \frac{1}{N_y} \right) \; \boldsymbol{H}_0. && \text{(B.32)} \end{aligned}$$

Transforming the magnetic intensity expression to prolate spheroidal coordinates yields

$$\boldsymbol{H}_0 = N_y \, M_y \left(\frac{\eta \cos\left(\phi\right) \sqrt{\xi^2 - 1}}{\sqrt{\xi^2 - \eta^2}} \; \hat{\boldsymbol{a}}_\eta - \frac{\xi \cos\left(\phi\right) \sqrt{1 - \eta^2}}{\sqrt{\xi^2 - \eta^2}} \; \hat{\boldsymbol{a}}_\xi + \sin\left(\phi\right) \; \hat{\boldsymbol{a}}_\phi \right). \tag{B.33}$$

Inspecting the general solution, setting $m = 1, n = 1$, $e_1 = 0$ and $f_1 = 1$ will generate the correct functional form of the magnetic intensity to satisfy the boundary conditions. With these settings the general solution simplifies to

$$\psi_1 = b_1 \left(\frac{\xi}{\sqrt{\xi^2 - 1}} - \frac{1}{2} \sqrt{\xi^2 - 1} \ln\left(\frac{\xi + 1}{\xi - 1} \right) \right) \sqrt{1 - \eta^2} \cos\left(\phi\right). \tag{B.34}$$

The remaining unknowns b_1 and N_y are determined by matching the two boundary conditions. Solving the two simultaneous equations yields the transverse demagnetizing factor

$$N_y = \frac{1}{2} \xi_0^2 - \frac{1}{4} \xi_0 \left(\xi_0^2 - 1 \right) \ln\left(\frac{\xi_0 + 1}{\xi_0 - 1} \right) \tag{B.35}$$

and

$$b_1 = c \, \xi_0 M_y \left(\xi_0^2 - 1 \right). \tag{B.36}$$

The expressions for $\boldsymbol{B}$ and $\boldsymbol{H}$ both inside and outside the prolate spheroid are now known. For the magnetic intensity outside of the spheroid we arrive at

$$\begin{aligned}\boldsymbol{H}_1 &= M_y\xi_0\left(\xi_0^2-1\right)\left\{\frac{\eta\cos\left(\phi\right)\sqrt{1-\eta^2}}{\left(\xi^2-\eta^2\right)\sqrt{\xi^2-1}}\,\hat{\boldsymbol{a}}_x\right.\\ &\quad+\left(\frac{1}{4}\ln\left(\frac{\xi+1}{\xi-1}\right)+\frac{\xi\cos\left(2\phi\right)}{2\left(\xi^2-1\right)}-\frac{\xi\cos^2\left(\phi\right)}{\xi^2-\eta^2}\right)\,\hat{\boldsymbol{a}}_y\\ &\quad\left.+\frac{\xi\cos\left(\phi\right)\sin\left(\phi\right)\left(1-\eta^2\right)}{\left(\xi^2-\eta^2\right)\left(\xi^2-1\right)}\,\hat{\boldsymbol{a}}_z\right\}.\end{aligned}\tag{B.37}$$

In a similar fashion, when the magnetization is directed along the z-direction, we find that the the demagnetizing factor is the same $N_z = N_y$, and that the magnetic intensity outside of the spheroid is

$$\begin{aligned}\boldsymbol{H}_1 &= M_z\xi_0\left(\xi_0^2-1\right)\left\{\frac{\eta\sin\left(\phi\right)\sqrt{1-\eta^2}}{\left(\xi^2-\eta^2\right)\sqrt{\xi^2-1}}\,\hat{\boldsymbol{a}}_x+\frac{\xi\cos\left(\phi\right)\sin\left(\phi\right)\left(1-\eta^2\right)}{\left(\xi^2-\eta^2\right)\left(\xi^2-1\right)}\,\hat{\boldsymbol{a}}_y\right.\\ &\quad\left.+\left(\frac{1}{4}\ln\left(\frac{\xi+1}{\xi-1}\right)-\frac{\xi\cos\left(2\phi\right)}{2\left(\xi^2-1\right)}-\frac{\xi\sin^2\left(\phi\right)}{\xi^2-\eta^2}\right)\,\hat{\boldsymbol{a}}_z\right\}.\end{aligned}\tag{B.38}$$

Which can also be obtained from (B.37) by interchanging y and z and noting $\phi \to \pi/2 - \phi$.

By superposition a spheroid with uniform and arbitrarily oriented magnetization in (x, y, z) can be created by summing the results of (B.28), (B.37) and (B.38).

B.5 Prolate spheroid in an uniform magnetic field

When a prolate spheroid with linear and isotropic magnetic properties is placed in an uniform magnetic field, magnetization proportional to the magnetic intensity is induced within the spheroid, this induced magnetization can be represented as

$$\boldsymbol{M}_i = \chi_m \boldsymbol{H}_0 \tag{B.39}$$

where χ_m is the magnetic susceptibility a dimensionless constant, and $\boldsymbol{H}_0$ is the magnetic intensity inside the spheroid. Assuming the applied magnetic intensity $\boldsymbol{H}_a$, is directed along the longitudinal axis of the spheroid, the magnetic intensity inside the spheroid can be written as

$$\boldsymbol{H}_0 = \boldsymbol{H}_a - N_x \boldsymbol{M}_i, \tag{B.40}$$

where N_x is the same longitudinal demagnetizing factor determined above. In terms of the applied field, the induced magnetization can now be expressed as

$$\boldsymbol{M}_i = \frac{\chi_m}{1+\chi_m N_x}\boldsymbol{H}_a. \tag{B.41}$$

The magnetic field inside the spheroid can be determined using (B.4), with $\boldsymbol{M} = \boldsymbol{M}_i$, which yields

$$\boldsymbol{B}_0 = \mu_\circ\left(1+\chi_m\right)\boldsymbol{H}_0. \tag{B.42}$$

Outside the spheroid (B.28) with $\boldsymbol{M} = \boldsymbol{M}_i$ is used.

When the applied field is in the y-direction the induced magnetization is given as

$$\boldsymbol{M}_i = \frac{\chi_m}{1 + \chi_m N_y} \boldsymbol{H}_a, \tag{B.43}$$

where N_y is the transverse demagnetizing factor, and the field intensity outside the spheroid is found using either (B.37). A similar result is obtained when the applied field is along z-direction.

By superposition any combination of transverse and longitudinal applied fields can be added together to allow the prolate spheroid to be arbitrarily oriented in an uniform magnetic field.

B.6 Combined induced and permanent magnetization

When considering a prolate spheroid with both permanent and induced magnetization we can compute the total magnetization as

$$\boldsymbol{M} = \boldsymbol{M}_p + \boldsymbol{M}_i, \tag{B.44}$$

where $\boldsymbol{M}_p$ is the permanent magnetization and $\boldsymbol{M}_i$ is the induced magnetization. When the permanent magnetization and applied field are expressed as vectors in cartesian coordinates as $\boldsymbol{M}_p = M_{px}\,\hat{\boldsymbol{a}}_x + M_{py}\,\hat{\boldsymbol{a}}_y + M_{pz}\,\hat{\boldsymbol{a}}_z$ and $\boldsymbol{H}_a = H_{ax}\,\hat{\boldsymbol{a}}_x + H_{ay}\,\hat{\boldsymbol{a}}_y + H_{az}\,\hat{\boldsymbol{a}}_z$, the resulting total magnetization is given as

$$\boldsymbol{M} = \left(M_{xp} + \frac{\chi_m}{1 + \chi_m N_x} H_{ax}\right) \hat{\boldsymbol{a}}_x + \left(M_{yp} + \frac{\chi_m}{1 + \chi_m N_y} H_{ay}\right) \hat{\boldsymbol{a}}_y + \left(M_{zp} + \frac{\chi_m}{1 + \chi_m N_z} H_{az}\right) \hat{\boldsymbol{a}}_z. \tag{B.45}$$

Where each component of the magnetization is used in (B.28), (B.37) and (B.38), respectively.

It is also feasible to have the magnetic susceptibility vary for each cartesian dimension. Another adaption is to treat the vertical magnetization as a constant (i.e. no induced term) since the applied vertical field is often constant, at least in studies related to a ship measured at a single location.

B.7 Superposition of magnetized spheroids

Adding together the field equations of multiple arbitrarily oriented and positioned spheroids is valid for the case where the magnetization of each spheroid is permanent.

The superposition principle does not apply for the case where induced magnetization is determined in the external field of a magnetized prolate, since the field is not uniform. Mathematically, the field induced by multiple spheroids in an uniform field, can always be summed.

This page intentionally left blank.

Annex C: AUV noise removal process

Assume the total-field magnetic noise from the REMUS vehicle is due to permanent magnetization, induced magnetization, eddy currents in the conductors, or constant electrical currents. These are the same assumptions that are used in aircraft noise reduction (Ref 7), so we can model the REMUS manoeuvre noise, as a function of time, as follows:

$$\text{Model}(t) = \sum_{i=1}^{18} C_i A_i(t) \qquad \text{(C.1)}$$

where C_i are constant coefficients and

$$\begin{aligned}
A_1 &= T / H_e \\
A_2 &= L / H_e \qquad \text{perm and constant currents} \\
A_3 &= V / H_e \\
\\
A_4 &= T \times T / H_e \\
A_5 &= T \times L / H_e \\
A_6 &= T \times V / H_e \qquad \text{induced} \\
A_7 &= L \times L / H_e \\
A_8 &= L \times V / H_e \\
A_9 &= V \times V / H_e \qquad \text{(C.2)} \\
\\
A_{10} &= (\partial T / \partial t) \times T / H_e \\
A_{11} &= (\partial T / \partial t) \times L / H_e \\
A_{12} &= (\partial T / \partial t) \times V / H_e \\
A_{13} &= (\partial L / \partial t) \times T / H_e \\
A_{14} &= (\partial L / \partial t) \times L / H_e \qquad \text{eddy currents} \\
A_{15} &= (\partial L / \partial t) \times V / H_e \\
A_{16} &= (\partial V / \partial t) \times T / H_e \\
A_{17} &= (\partial V / \partial t) \times L / H_e \\
A_{18} &= (\partial V / \partial t) \times V / H_e \quad .
\end{aligned}$$

Here (T,L,V) are the time-series outputs of a vector magnetometer that measures the components of the Earth's field and thus the orientation of the REMUS vehicle as it manoeuvres, and

$$H_e = \sqrt{T^2 + L^2 + V^2} \quad . \qquad \text{(C.3)}$$

Note we can also build up the model from the pitch, roll, and heading angle measurements, but it has this particularly simple form if we use vector magnetometer outputs.

The coefficients (C_i) can be obtained by doing a least-squares fit of the terms (A_i) to the measured TF signal over some segment of data. Theoretically those calculated coefficients C_i could be used to reduce vehicle manoeuvre noise on any other data collected with the REMUS vehicle (on a different day, on all headings, at all depths, etc). However, the calculation of those coefficients can be dramatically affected by several things, including other sources of noise on TF (for instance geology, geomagnetic variations, etc). To ensure that the coefficients we derive are related to the actual manoeuvres of the REMUS and not to these other noise sources, we apply a bandpass filter to the measured TF and A_i before the least squares-fitting is done. The edges of the bandpass filter are related to the known manoeuvre frequencies. Now the noise model is

$$\text{Filtered}\{\text{Model}(t)\} = \sum_{i=1}^{18} C_i \times \text{Filtered}\{A_i(t)\} \qquad \text{(C.4)}$$

and the coefficients C_i can be calculated with a least-squares fitting routine where the following quantity is minimized

$$\left| \text{Filtered}\{\text{TF}\} - \text{Filtered}\{\text{Model}\} \right|^2 . \qquad \text{(C.5)}$$

However, we are really interested in removing noise from the unfiltered TF, not just the filtered TF, because the prolate spheroid and dipole fitting algorithms will be applied to the unfiltered total-field data. To do this, take the calculated coefficients C_i, the measured unfiltered vector magnetometer signals (T,L,V) and use equation (C.1) to get the time series estimate of the unfiltered magnetic noise caused by REMUS manoeuvres. Now subtract the unfiltered model noise from the raw total-field measurements to get the compensated total-field (TFC)

$$\text{TFC}(t) = \text{TF}(t) - \text{Model}(t) . \qquad \text{(C.6)}$$

Finally, there may be a significant DC shift caused by this technique because some of the terms (notably V/H_e and $V \times V/H_e$) may not be zero-mean. To get around this, simply remove the mean from noise model prior to subtracting it from the raw total-field. i.e.

$$\text{TFC}(t) = \text{TF}(t) - \{ \text{Model}(t) - \langle \text{Model}(t) \rangle \} . \qquad \text{(C.7)}$$

Distribution list

Report #: DRDC Atlantic TM 2007-223
Title: Magnetic Source Parameters of *MR OFFSHORE* Measured During Trial MONGOOSE 07
Author: J. Bradley Nelson and Troy C. Richards
Date: September 2007
Classification: UNCLASSIFIED

List A (Full Report)
Internal

5 - Library
1 - Troy Richards
1 - GL/ISM

External

2 - DRDKIM
1 - Institute for Aerospace Research, Flight Research Laboratory
1200 Montreal Road, Ottawa. ON. K1A 0R6
Attn: J. Bradley Nelson
1 - Naval Surface Warfare Center – Panama City
110 Vernon Avenue, Panama City, FL 32407-7001
Attn: Mike Wynn, Ted Clem
1 - Office of Naval Research
One Liberty Center, 875 North Randolph Street, Arlington, VA 22217
Attn: Dana Hesse (Code 321), George Stimak (Code 331), Thomas Swean (Code 321OE)
1 - Naval Surface Warfare Center, Carderock Division
9500 MacArthur Blvd, W. Bethesda, MD 20817-5700
Attn: Don Pugsley, Bld 80
1 - Department of Defence
Mine Warfare Systems Group, 17 Pirrama Road, PO Box 44 Pyrmont, NSW 2009
Attn: Andrew Munyard

List B (Executive Summary Only)

External

2 - DRDC Corp
Attn: DSTA 5, DSTM

This page intentionally left blank.

DOCUMENT CONTROL DATA

(Security classification of title, body of abstract and indexing annotation must be entered when the overall document is classified)

1. ORIGINATOR (the name and address of the organization preparing the document. Organizations for whom the document was prepared, e.g. Centre sponsoring a contractor's report, or tasking agency, are entered in section 8.)

DRDC Atlantic

2. SECURITY CLASSIFICATION (overall security classification of the document including special warning terms if applicable).

UNCLASSIFIED

3. TITLE (the complete document title as indicated on the title page. Its classification should be indicated by the appropriate abbreviation (S,C,R or U) in parentheses after the title).

Magnetic Source Parameters of *MR OFFSHORE* Measured During Trial MONGOOSE 07

4. AUTHORS (Last name, first name, middle initial. If military, show rank, e.g. Doe, Maj. John E.)

Nelson, J. Bradley and Richards, Troy C.

5. DATE OF PUBLICATION (month and year of publication of document)	6a. NO. OF PAGES (total containing information Include Annexes, Appendices, etc).	6b. NO. OF REFS (total cited in document)
September 2007	35	8

7. DESCRIPTIVE NOTES (the category of the document, e.g. technical report, technical note or memorandum. If appropriate, enter the type of report, e.g. interim, progress, summary, annual or final. Give the inclusive dates when a specific reporting period is covered).

Technical Memorandum

8. SPONSORING ACTIVITY (the name of the department project office or laboratory sponsoring the research and development. Include address).

Defence R&D Canada – Atlantic
PO Box 1012
Dartmouth, NS, Canada B2Y 3Z7

9a. PROJECT OR GRANT NO. (if appropriate, the applicable research and development project or grant number under which the document was written. Please specify whether project or grant).	9b. CONTRACT NO. (if appropriate, the applicable number under which the document was written).
11CA03/11GS03	

10a ORIGINATOR'S DOCUMENT NUMBER (the official document number by which the document is identified by the originating activity. This number must be unique to this document.)	10b OTHER DOCUMENT NOs. (Any other numbers which may be assigned this document either by the originator or by the sponsor.)
DRDC Atlantic TM 2007-223	

11. DOCUMENT AVAILABILITY (any limitations on further dissemination of the document, other than those imposed by security classification)

(x) Unlimited distribution
( ) Defence departments and defence contractors; further distribution only as approved
( ) Defence departments and Canadian defence contractors; further distribution only as approved
( ) Government departments and agencies; further distribution only as approved
( ) Defence departments; further distribution only as approved
( ) Other (please specify): TTCP

12. DOCUMENT ANNOUNCEMENT (any limitation to the bibliographic announcement of this document. This will normally correspond to the Document Availability (11). However, where further distribution (beyond the audience specified in (11) is possible, a wider announcement audience may be selected).

13. ABSTRACT (a brief and factual summary of the document. It may also appear elsewhere in the body of the document itself. It is highly desirable that the abstract of classified documents be unclassified. Each paragraph of the abstract shall begin with an indication of the security classification of the information in the paragraph (unless the document itself is unclassified) represented as (S), (C), (R), or (U). It is not necessary to include here abstracts in both official languages unless the text is bilingual).

Sea mines can be triggered by the magnetic field from a naval vessel, and thus monitoring the magnetic state of a naval vessel is critical. The vessel's signature is usually measured by sailing it over an electromagnetic (EM) range equipped with bottom-mounted magnetic sensors. If the magnetic signature is too large, then some type of treatment (degaussing, de-perming, etc) is done to reduce it. Range facilities are often far from the vessel's operating area and require considerable transit time to reach them. "Forward EM ranging" is the term used for making EM signature measurements with portable sensors while the vessel is in the operating area.

One concept for locating and identifying sea mines is to use a combined sonar/magnetic detection system. The Naval Surface Warfare Center in Panama City, Florida (NSWC-PC) has developed such a system on a REMUS autonomous underwater vehicle (AUV). Because the REMUS magnetic sensor is also capable of measuring a naval vessel's signature, and its navigation system is capable of accurately measuring the AUV's position and orientation, then it should be possible to use their REMUS for forward EM ranging.

DRDC Atlantic and the NSWC-PC measured the magnetic signature of the vessel *MR OFFSHORE* using the laser scalar magnetic gradiometer-equipped REMUS underwater vehicle during trial MONGOOSE 07 in June 2007. The magnetic signatures were measured on a number of ship and REMUS headings. These data have been analysed to yield the permanent and induced magnetic parameters of *MR OFFSHORE*. Two different modeling techniques, one using dipole and quadrupoles, and another using a single prolate spheroid, were used and the results are consistent.

The prolate spheroid parameters were used to forward-model the 3-component signature of *MR OFFSHORE* during a pass near the DRDC Diver Signature Integrated Measurement System (DSIMS). The fit was quite close, and the estimated speed of the ship based on the fitting algorithm matched the captain's declared speed during the pass. This validates of the concept of using portable magnetic sensors for forward EM ranging.

14. KEYWORDS, DESCRIPTORS or IDENTIFIERS (technically meaningful terms or short phrases that characterize a document and could be helpful in cataloguing the document. They should be selected so that no security classification is required. Identifiers, such as equipment model designation, trade name, military project code name, geographic location may also be included. If possible keywords should be selected from a published thesaurus. e.g. Thesaurus of Engineering and Scientific Terms (TEST) and that thesaurus-identified. If it not possible to select indexing terms which are Unclassified, the classification of each should be indicated as with the title).

magnetic signatures
magnetic modeling
forward ranging

This page intentionally left blank.

Defence R&D Canada

Canada's leader in defence
and National Security
Science and Technology

R & D pour la défense Canada

Chef de file au Canada en matière
de science et de technologie pour
la défense et la sécurité nationale

www.drdc-rddc.gc.ca